Predicting different components of blast-induced ground vibration using earthworm optimisation-based adaptive neuro-fuzzy inference system

Hoang Nguyen, Yosoon Choi, Masoud Monjezi, Nguyen Van Thieu & Trung-Tin Tran

Published online: 18 Sep 2023.

Submit your article to this journal 🗗

View related articles 🗗

View Crossmark data 🗗

Taylor & Francis
Taylor & Francis Group

Check for updates

Predicting different components of blast-induced ground vibration using earthworm optimisation-based adaptive neuro-fuzzy inference system

Hoang Nguyen [a,b], Yosoon Choi[c], Masoud Monjezi[d], Nguyen Van Thieu[e] and Trung-Tin Tran[f]

[a]Department of Surface Mining, Mining Faculty, Hanoi University of Mining and Geology, Hanoi, Vietnam; [b]Innovations for Sustainable and Responsible Mining (ISRM) Research Group, Hanoi University of Mining and Geology, Hanoi, Vietnam; [c]Department of Energy Resources Engineering, Pukyong National University, Busan, Republic of Korea; [d]Faculty of Engineering, Tarbiat Modares University, Tehran, Iran; [e]Faculty of Computer Science, Phenikaa University, Hanoi, Yen Nghia, Ha Dong, Vietnam; [f]Department of Information Technology, Swinburne University of Technology – FPT University, Da Nang, Vietnam

ABSTRACT

This study focuses on addressing the complexity inherent in various amplitude components of blast-induced ground vibration (BIGV), encompassing vertical, radial, transversal, and the vectoral sum of PPVs of particle velocity. It takes into account their nonlinearity across diverse quarry environments, and aims to present an enhanced nonlinear intelligent system for accurate prediction of these components. Multiple artificial intelligence models were explored and developed for this purpose, including a support vector machine (SVM), an adaptive neural network based on the fuzzy inference system (ANFIS), and a novel hybrid model that combines earthworm optimisation (EO) and ANFIS (EO-ANFIS). The study also leverages the empirical model offered by the United States Bureau of Mines. The outcomes highlighted that the predictions of the three individual components prove to be more accurate compared to the vectoral sum of PPVs of particle velocity. However, the latter remains a valuable metric for evaluating the magnitude of BIGV in open-pit mines. Notably, the hybrid EO-ANFIS model emerges as the most accurate, achieving an impressive ~ 75% accuracy across 10 quarries characterised by distinct geological conditions.

1. Introduction

In open pit mining, the fragmentation of hard rocks is commonly achieved through blasting, owing to its cost-effectiveness and potent results, despite its notable economic and technical merits. Nonetheless, the potential negative repercussions of mine blasting on the surrounding environment have garnered substantial attention from state regulatory bodies, mining enterprises, and the scientific realm. These concerns encompass various factors, such as ground vibration (BIGV), air blasts, flyrock, dust, and harmful substances.

Among these factors, BIGV emerges as a foremost issue, with its impact evaluated using peak particle velocity (PPV). The apprehension surrounding this matter is amplified by the considerable damage it can cause to structures, residences, bench groupings, and slopes [1–3].
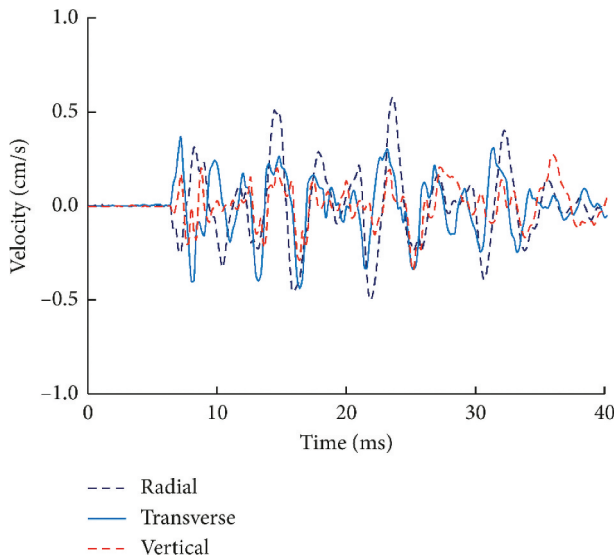
Figure 1. Illustration of PPV components of a borehole [4].

When blast-induced ground vibrations are induced, particle movement occurs in three dimensions, and we measure these motions through specific components. These components encompass:

1. Radial or longitudinal: This component involves movement from the front to the back, aligned with the direction of wave propagation. It signifies the oscillation of particles in a direction parallel to the wave's travel.

2. Vertical: This component entails movement in an upward and downward direction, perpendicular to the wave's propagation. It represents the vertical displacement of particles as the wave passes through.

3. Transverse: In the case of the transverse component, particles move from side to side, perpendicular to both the wave's direction and the vertical component. This kind of motion characterises waves where the oscillations are at right angles to the direction of wave travel.

These components and their associated wave types help us comprehend the intricate nature of particle motion and wave propagation during events like blast-induced ground vibrations Figure 1.

To control PPV, scholars have proposed various empirical formulas based on historical blasts [5]. Accordingly, the empirical equations were determined based on the mechanical and geological properties. Amongst, most of them are based upon the scaled distance between the explosive charged (W) and monitoring distance (D) [6–10]. In addition, Kumar, Choudhury and Bhargava [5] considered the rock properties to establish an empirical equation for predicting PPV. Nevertheless, previous researchers' results and recommendations indicated that the empirical equations' performance and accuracy might be varied or poorer in different areas due to the complex geological and geophysical conditions [11–15].

Lately, there has been a focus on employing cutting-edge methods like artificial intelligence (AI) for accurate PPV prediction in competitive settings. A noteworthy example is the work by Amiri, Amnieh, Hasanipanah and Khanli [16], who devised a novel approach. They fused an artificial neural network (ANN) with the k-nearest neighbour algorithm to forecast PPV at an Iranian dam. Impressively, their model achieved a remarkable determination coefficient (R^2) of 0.88, the highest reported so far. In another study, Hasanipanah, Faradonbeh, Amnieh, Armaghani and Monjezi [17] incorporated an additional machine learning approach utilising a decision tree model, specifically the Classification and Regression Trees (CART), to forecast the PPV resulting from blasting activities at an Iranian copper mine. This model achieved

a remarkable R^2 value of 0.95, demonstrating its high predictive accuracy. Shang, Nguyen, Bui, Tran and Moayedi [18] harnessed AI technology employing the ANN model, fine-tuned by the firefly optimisation algorithm (FFA), achieving an impressive R^2 of 96.6 in forecasting PPV at a Vietnamese quarry. Similarly, Chen, Hasanipanah, Rad, Armaghani and Tahir [19] introduced a variety of hybrid models by combining ANN, support vector machine (SVM), and optimisation algorithms, such as FFA, PSO (particle swarm optimisation) [20], and GA (genetic algorithm) [21], to anticipate PPV. Their investigation revealed FFA-SVM as the optimal data-driven model for this purpose. Arthur, Temeng and Ziggah [22] employed the Gaussian programming (GP) method to remarkably precise PPV predictions.

Innovative hybrid approaches blending the extreme gradient boosting (XGBoost) and optimisation techniques such as grey wolf optimisation (GWO) [23], whale optimisation algorithm (WOA) [24], and biological optimisation (BO) [25] have been devised as cutting-edge models for PPV prediction [26]. Additionally, an ANN model rooted in gradient boosted trees (GBT) demonstrated its efficacy in PPV prediction due to its simplicity and reliability.

Furthermore, a range of other research initiatives have proposed AI-based models with favourable outcomes for PPV prediction [27–39]. Over the past two decades, numerous AI-based models have emerged, with as many as 12 novel hybrid models specifically for PPV prediction introduced in 2021 (as cited in references [27–39]). This surge in research activity underscores the ongoing global concern among researchers regarding accurate PPV prediction.

An analysis of existing literature underscores the significance of PPV prediction within the mining domain, where numerous AI models showcasing promising outcomes have been introduced for this subject. Recent articles, however, have frequently directed their attention towards hybrid models, asserting that these hybrids can yield higher levels of accuracy compared to conventional models. Nevertheless, there remains a trove of unexplored hybrid models that might hold superior potential.

Furthermore, the majority of prior investigations have exclusively addressed the summation vector of PPV, disregarding the breakdown of its amplitude components, which include vertical PPV, transversal PPV, and radial PPV. Stated differently, preceding studies have concentrated solely on predicting the PPV peak point among the three mentioned constituents. This signifies that the peak point could be located within the vertical PPV, transversal PPV, or radial PPV. However, there are instances where the peak points are not located in the directions of wave propagation. This misalignment could significantly impact the structures near the blasting site. Consequently, in cases where the peak points are not located in wave propagation directions, the prediction of the normal PPV (peak point) and its accuracy are not meaningful. In addition, the application of AI models for PPV prediction has predominantly focused on single study sites, with scant attention given to extending predictions to encompass diverse regions, as seen in only a handful of studies involving multiple mines (e.g. three or four mines) [40,41].

Furthermore, the AI models developed or proposed thus far have exhibited limited generalisability across different sites, and their true capabilities remain underexplored. To address these limitations, this study embarks on the following innovations:

- The amplitude components, including vertical PPV, transversal PPV, radial PPV, and the Vectoral sum of PPVs, are treated as distinct entities and predicted individually utilising AI techniques.
- Drawing from datasets collected from 10 quarries situated in various locations across Nigeria, the goal is to predict distinct amplitude components through a comprehensive intelligent model.
- Introducing the innovative EO-ANFIS model (earthworm optimisation – adaptive neuro-fuzzy inference system) as a means to forecast PPV amplitude components.
- A comparative analysis is undertaken, contrasting the proposed hybrid EO-ANFIS model with ANFIS (without optimisation), SVM, and empirical models in their respective predictions of PPV amplitude components.

The choice of the ANFIS algorithm for hybridisation in predicting PPV resulting from mine blasting is rooted in a careful consideration of several factors. While there are indeed more robust machine learning (ML) algorithms available, the decision to employ ANFIS was based on a deliberate evaluation of the specific needs and characteristics of our prediction task, as well as the strengths of ANFIS in addressing those requirements.

ANFIS is particularly suited for this task due to its inherent ability to handle complex and non-linear relationships within the data. The prediction of PPV in mine blasting involves intricate interactions between various parameters, such as blast design, geological conditions, and explosive properties, resulting in a dataset characterised by non-linear dependencies. ANFIS excels in capturing these intricate relationships through its fusion of fuzzy logic and neural networks, allowing it to model the intricacies of PPV generation more effectively compared to traditional ML algorithms.

Furthermore, ANFIS has the advantage of being interpretable. This is crucial in the context of mining and geology, where understanding the underlying factors contributing to PPV is of paramount importance. The transparency of ANFIS enables us to gain insights into how different input parameters influence the PPV outcomes, aiding in informed decision-making during blast design and site management.

While other ML algorithms might exhibit greater complexity or attain higher predictive accuracy in specific scenarios, ANFIS strikes a balance between accuracy and interpretability that aligns well with the requirements of this study. Additionally, there exists a plethora of ML algorithms and neural networks, creating a challenge in determining which algorithm or model is optimal. The most effective approach for tackling this task involves the utilisation of the 'trial and error' method. In this study, the ANFIS model was specifically trial, and its integration with the EO optimisation algorithm was investigated. This combination empowers us to craft a model that not only delivers precise predictions but also provides insights into the underlying dynamics. As a result, it emerges as a valuable tool for enhancing both the safety and efficiency of mine blasting operations.

2. Methodology

2.1. Earthworm optimisation (EO)

EO is a swarm-based metaheuristic algorithm proposed by Wang, Deb and Coelho [42], inspired by the behaviours of earthworms in nature. The EO can adopt optimisation problems based on the following behaviours:

- Every earthworm can produce offspring with two types of reproduction.
- The generated baby earthworms hold all the genes and length of their parents.
- Operators cannot alter the earthworm singular with the best fitness permit on straight next generation. Thus, the earthworm populations can increase in the generations.

For producing offspring, earthworms can carry out the two following ways:

Reproduction 1: The baby earthworm can be born by a single parent based on the hermaphrodite's mechanism. This reproduction is characterised by the position of the earthworm (P), and the mathematical formula is described in Equation (1):

$$P_{i_1,n} = P_{\max,n} + P_{\min,n} - \eta P_{i,n} \tag{1}$$

where i_1 is the ith earthworm in the reproduction 1; n is the number of earthworms; η denotes the distance between the child and its parent, which is characterised by the similarity factor. When $\eta = 0$, the algorithm implements a local search and $\eta = 1$, it will implement a global search.

Reproduction 2: Suppose that the EO includes S generated offsprings with $S = 1, 2, \ldots n$. The position of the earthworm can be calculated using Equation (2):

$$P_{i_2} = \sum_{n=1}^{S} w_n P_{S,n} \tag{2}$$

with w_n is the weight of offspring, and it can be determined using Equation (3):

$$w_n = \frac{1}{S-1} \frac{\sum\limits_{j=1,j\neq n}^{S} f_j}{\sum\limits_{j=1}^{S} f_j} \tag{3}$$

$$= \frac{1}{S-1} \frac{f_1 + f_2 + \ldots + f_{n-1} + f_{n+1} + \ldots + f_{S-1} + f_S}{f_1 + f_2 + \ldots + f_{n-1} + f_n + f_{n+1} + \ldots + f_{S-1} + f_S}$$

where f_j is the fitness of the jth offspring.

Once the EO implements two types of reproduction, the position of the ith earthworm in the next generation is determined as follows:

$$P_i' = \beta P_{i_1} + (1 - \beta) P_{i_2} \tag{4}$$

where β denotes the proportional coefficient of P_{x_1} and P_{x_2}, and it is described as follows:

$$\beta^{t+1} = \gamma \beta^t \tag{5}$$

where t stands for the current generation of earthworm; γ is the cooling factor that was proposed by Kirkpatrick, Gelatt and Vecchi [43].

Mathematical model of the EO algorithm for optimisation problems is presented in Figure 2.

2.2. Anfis

ANFIS is a type of ANN that combines the fuzzy inference system (FIS). ANN extricates the fuzzy rules and membership functions based on the input information. This way, ANFIS can explain the complex relationships of the attributes in the dataset using learning algorithms. ANFIS is a multi-layer feedforward network developed based on five layers [44], as shown in Figure 3. Whereas the fuzzification and defuzzification layers have adaptive nodes, the nodes in the other layers are fixed. The FIS of ANFIS has a higher reasoning ability level using the IF-THEN rules as a knowledge base [45]. Through these rules and five layers, the inputs $x_1, x_2, \ldots x_m$ from the dataset are forwarded and calculated errors.

The rule of the ANFIS can be described as follows:

Suppose that the ANFIS structure has n input variables (i.e. $x_1, x_2, \ldots x_n$), the corresponding fuzzy sets are $A_j, B_j, \ldots C_j$. The output inside the defined fuzzy rule is defined as follows:

$$S_j = a_j x_1 + b_j x_2 + \ldots + c_j x_n + g_j \tag{6}$$

where $a_j, b_j, \ldots c_j, g_j$ are specified parameters of the training process.

Layer 1 now can be calculated as follows:

$$L_{1,j} = \lambda_{A_1} x_1, L_{1,j} = \lambda_{B_1} x_2, L_{1,j} = \lambda_{C_1} x_n \tag{7}$$

where $\lambda_{A_1} x_1, \lambda_{B_1} x_2, \lambda_{C_1} x_n$ are selected to obtain bell-shaped with the interval [0,1], and they can be determined using Equation (8):

$$\lambda_{A_1} x_1 = \lambda_{B_1} x_2 = \lambda_{C_1} x_n = \left(\frac{1}{1 + \left(\frac{x - r_j}{k_j} \right)^{2z_j}} \right) \tag{8}$$

Algorithm: Earthworm optimization pseudo-code
1	Generate initial parameters: generation, population (*NP*), number of the kept earthworms *nKEW*, maximum number of generations (*MaxGen*), similarity factor, initial proportional coefficient, cooling factor.
2	Evaluating the fitness of earthworms
3	**While** the best solution is not found or
4	$t < MaxGen$ **do**
5	Sort all the earthworm individuals according to their fitness.
6	**For** $i = 1$ to *NP* **do**
7	// Implement reproduction 1
8	Generate P_{x1}
9	// Implement reproduction 2
10	**If** I > *nKEW* **then**
11	Define the number of selected parents (*N*) and generated offsprings (*S*)
12	Select *N* parents by using roulette wheel selection
13	Generate S offsprings
14	Computing P_{i2} according to the generated offsprings S in Eq. (2)
15	**Else**
16	**End while**
17	Save the best solution
18	**End.**

Figure 2. The EO's pseudo code.

where r_j, k_j, z_j denote the set of parameters.

Layer 2 is calculated using Equation (9):

$$L_{2,j} = wp_j = \lambda_{A_1} x_1 \times \lambda_{B_1} x_2 \times \lambda_{C_1} x_n, j = 1, 2 \tag{9}$$

where p_j is the jth rule firing strength of the second layer.

Layer 3 is calculated using Equation (10):

$$L_{3,j} = \frac{wp_j}{(wp_1 + wp_2)}, j = 1, 2 \tag{10}$$

Layer 4 is calculated as follows:

$$L_{4,j} = wp_j S_j, j = 1, 2 \tag{11}$$

Layer 5 is calculated as follows:

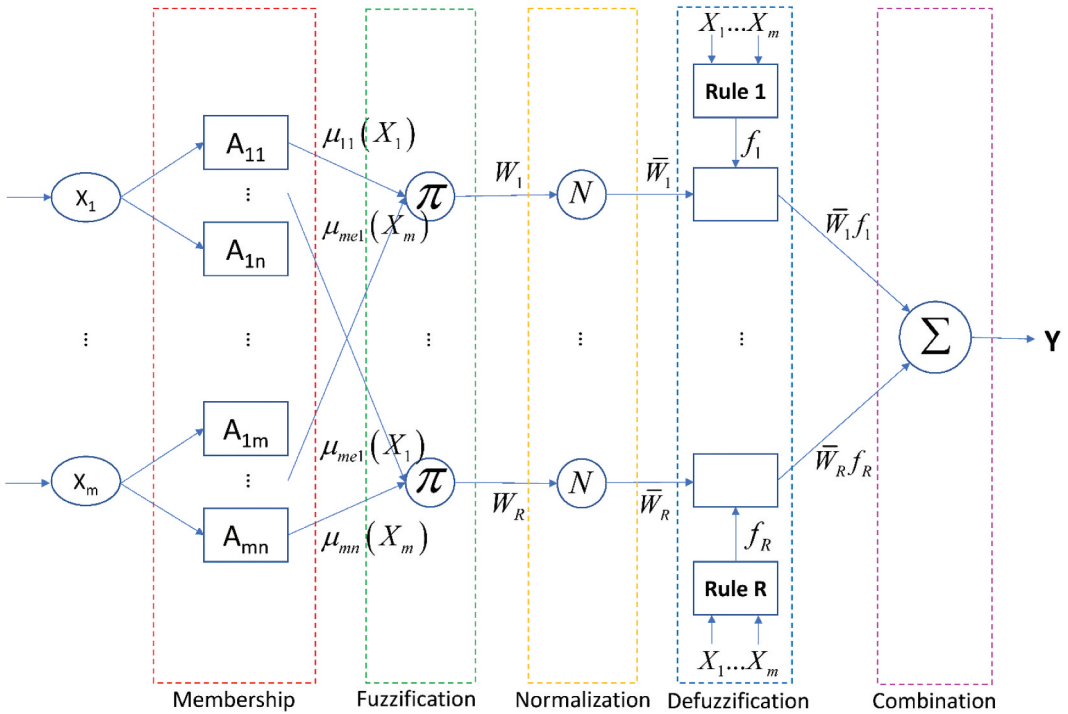$$L_{5,j} = \frac{\sum_{j=1}^{n} wp_j S_j}{\sum_{j=1}^{n} wp_j} \tag{12}$$

Figure 3. Architecture of the general ANFIS network.

Finally, the output of the ANFIS model is calculated based on the predefined threshold value ε, as follows:

$$output = \begin{cases} error, & Y < \varepsilon \\ no\, error, & Y \geq \varepsilon \end{cases} \tag{13}$$

More details of the ANFIS model can be found in the literature [46–50].

2.3. EO-ANFIS

For training the ANFIS model, the following algorithms were often used to adjust the parameters of the membership functions, such as backpropagation, gradient descent, and Runge-Kuta [51]. However, early convergence and being stuck in the local optima often occur for these algorithms, and the ANFIS model might not achieve global optimal. Therefore, optimisation algorithms can be potential solutions in this regard. Herein, the EO algorithm was used as an alternative training algorithm to train the ANFIS model, aiming to overcome the mentioned disadvantages of the traditional training algorithms.

Accordingly, the EO algorithm generates several solutions based on the optimisation mechanisms of the earthworms. For training the ANFIS model, each generated solution is a set of weights for the membership function used. They are embedded in the network to predict PPV amplitude components. The number of solutions depends on the number of populations initialised before running the algorithm. RMSE was used as the objective function for each solution, and RMSE was calculated to evaluate the model's fitness. The calculation is repeated with several iterations to determine the best fitness of the model (i.e. the lowest RMSE). Finally, the optimal EO-ANFIS model predicts PPV amplitude components, as shown in Figure 4.
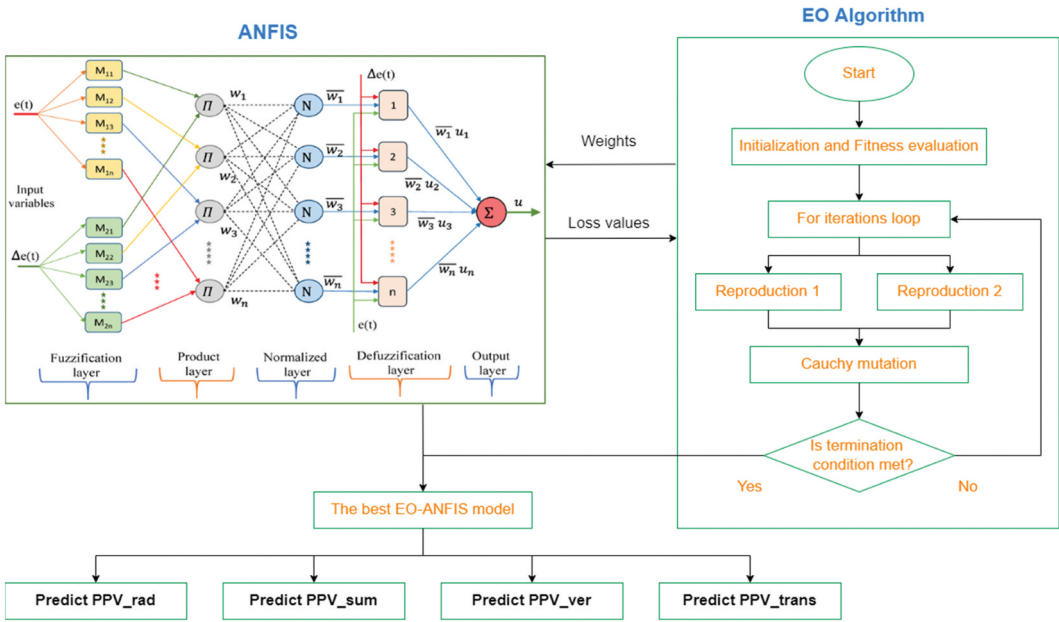
Figure 4. Proposing the EO-ANFIS framework for predicting PPV amplitude components.

3. Materials

To develop a generalised model to predict PPV amplitude components using the proposed EO-ANFIS framework, this study considered the PPV datasets collected from 10 various quarries in Nigeria. These quarries are located in the Abeokuta and Ibadan areas, as shown in Figure 5, and some quarries are shown in Figure 6. The dataset is available in Hammed, Popoola, Adetoyinbo, Awoyemi, Adagunodo, Olubosede and Bello [52]. However, the authors only evaluated the PPV components for each mine separately based on an empirical method.

In the Abeokuta and Ibadan areas, rock mass properties are pretty complex. The saturated-surface-dry mass is in the range of 80–130 grams; the saturated-submerged mass is in the range of 60–100; the density is in the range of 2.0 to 3.0 g/cm³; the porosity is the interval [1.5, 3.0], uniaxial compressive strength (UCS) is in the range of 121.1 MPa to 400 MPa, and shear strength is in the range of 60.5 to 92.6 MPa.

For each quarry, we compiled data from 20 blasting patterns, including values for width (W), burden (D), vertical PPV (PPV_ver), transversal PPV (PPV_trans), radial PPV (PPV_rad), and the vectoral sum of PPVs (PPV_sum). The distance between blasting sites and residential buildings was determined using GPS devices. To monitor the amplitude components of PPV, a seismograph (specifically, the V9000 from Vibrock Limited) was employed.

The primary explosive used for rock fragmentation in these quarries is Ammonium Nitrate Fuel Oil (ANFO). As a result, we collected a total of 200 blasting events across 10 quarries, encompassing various geographical regions. It's crucial to recognise that geological conditions can significantly differ between areas in mining and geology. Therefore, our dataset, containing 200 blasting events from diverse quarries, stands as a comprehensive and generalised representation suitable for various quarry settings.

We've summarised the statistical aspects of this dataset in Table 1, while the finer details are visually depicted in Figure 7. Among the parameters listed in Table 1, D and W were designated as input variables, while the remaining parameters were designated as output variables.
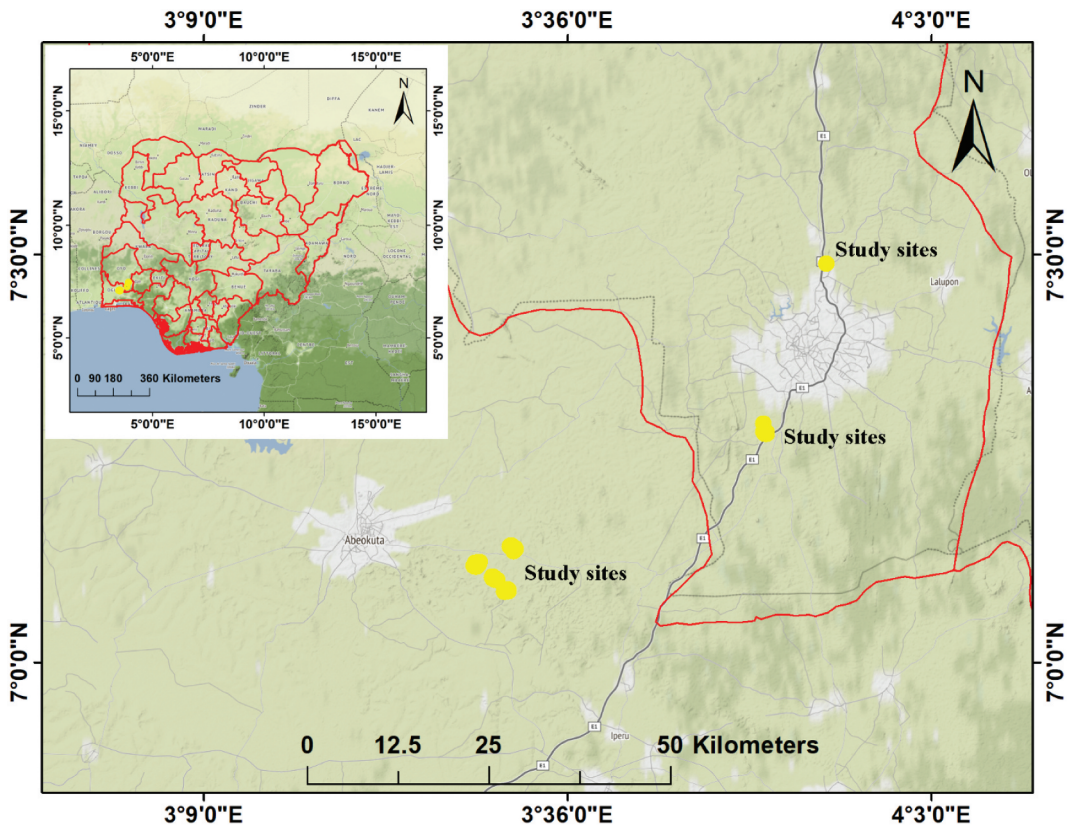
Figure 5. Major quarry sites in the field surveys.

4. Results and discussion

4.1. ANFIS model

For predicting PPV amplitude components by the ANFIS model, the dataset was normalised using the MinMax scaling method interval [0,1] to improve the accuracy and the learning rate of the ANFIS model. Next, 160 blasting events (~80%) were randomly selected to develop the ANFIS model, and the remaining 40 blasting events were used to test the accuracy of the developed ANFIS model. The Gaussian membership functions (MFs) were used for valuation extension. To train the ANFIS model, the stochastic gradient descent (SGD) algorithm was utilised. The ANFIS model's performance was assessed using a 10-fold cross-validation technique, with the goal of preventing the occurrence of overfitting issues.

Herein, the ANFIS model was designed with four MFs, and RMSE was used to evaluate the error of the ANFIS model. The model was deployed within 1000 epochs. The training and testing performance curves, fuzzy memberships with errors, and the outcome predictions on the training dataset of the PPV amplitude components are shown in Figures 8,9,10,11.

4.2. EO-ANFIS model

To enhance the ANFIS model, the EO algorithm was applied to optimise ANFIS's weights. The optimised EO-ANFIS model was then used to predict PPV amplitude components. Besides, the same topology network of the ANFIS model was used and the EO optimised this structure by

Figure 6. Some quarries in the Abeokuta and Ibadan areas (source: internet).

Table 1. Summary of the PPV amplitude components.

Statistics	D	W	PPV_ver	PPV_rad	PPV_trans	PPV_sum
Min.	300	650	4.67	4.55	4.63	8
1st Qu.	537.5	1250	16.24	16.07	16.09	28.14
Median	775	1500	27.18	27	27.32	46.94
Mean	775	1518	37.23	37.13	37.04	64.17
3rd Qu.	1012.5	1800	48.69	48.4	48.19	83.9
Max.	1250	2950	142.91	142.94	142.89	247.53

generating solutions with optimised weights. Before the framework in Figure 4 is applied, the parameters of EO were initiated with the crossover = 0.9, mutation = 0.01, number of earthworms = 2, similarity factor = 0.98, proportional factor = 1 and cooling factor = 0.9. The EO-ANFIS model's performance was also assessed using a 10-fold cross-validation technique, like those used for the ANFIS model, with the goal of preventing the occurrence of overfitting issues.

Once the EO's parameters were established, the number of populations (i.e. earthworms) were generated with the different number of earthworms, such as 50, 100, 150, 200, 250, 300, 350, 400,
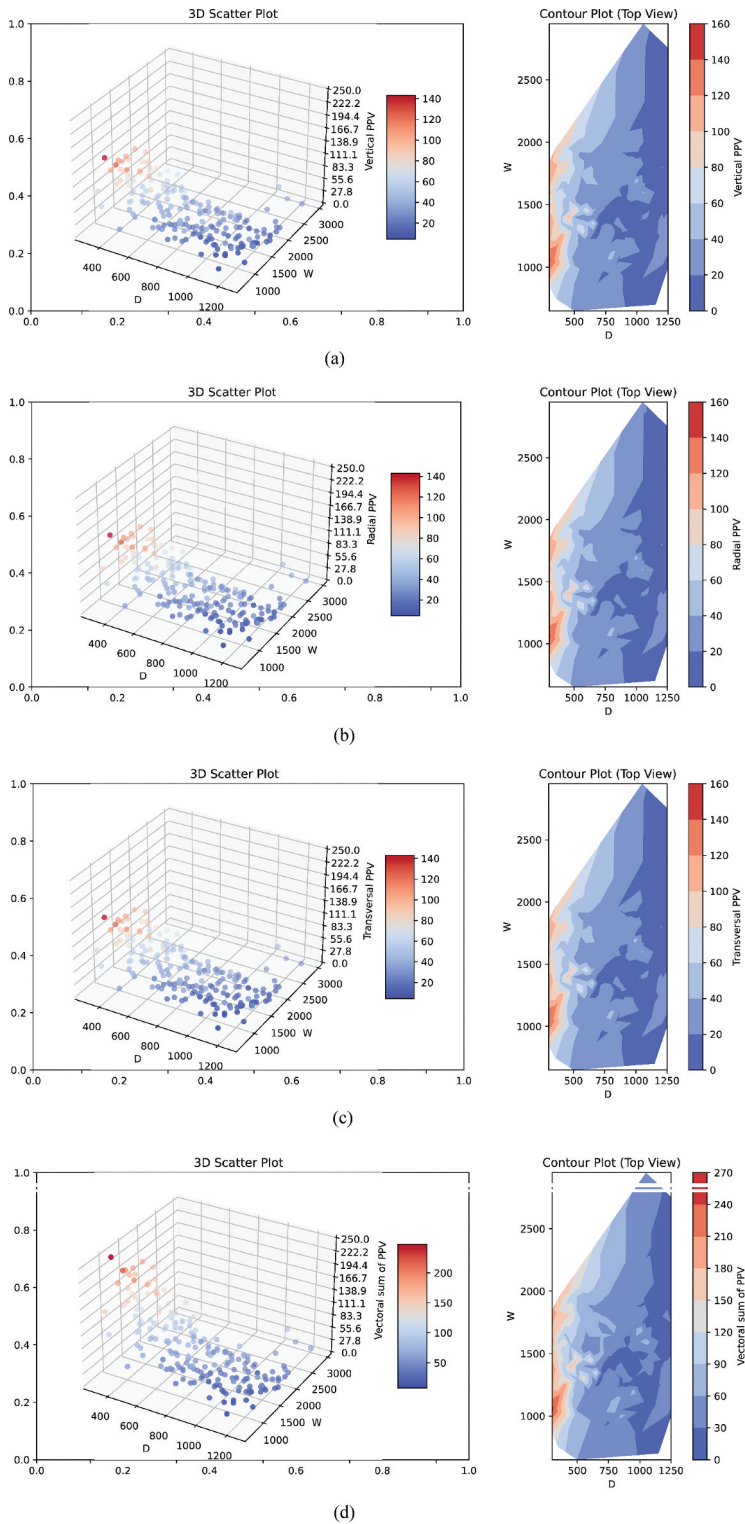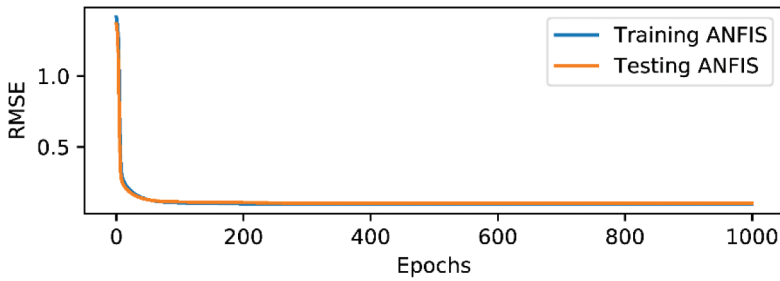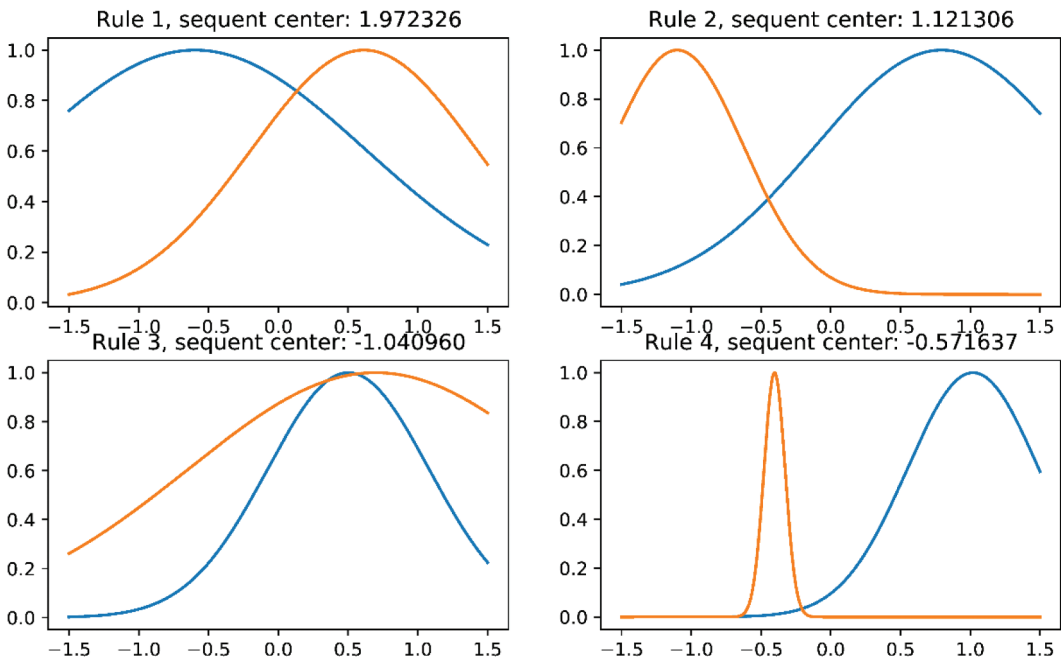
Figure 7. Plots of the dataset used (a) vertical PPV; (b) radial PPV; (c) transversal PPV; (d) vectoral sum of PPV.

(a)

(b)

Figure 8. Training performance and the accuracy of the ANFIS model for predicting vertical PPV (a) performance curves; (b) Trained MFs.

450, 500. RMSE was used to measure the error of the EO-ANFIS model during training progress. The EO algorithm then generated various sets of weights. They were then optimised and imported to the ANFIS model for predicting PPV amplitude components with 1000 iterations, as shown in Figure 12.

The training results in Figure 12 show that the EO algorithm seems to be very good in learning the errors of the ANFIS model, and the EO-ANFIS model's convergence is also excellent. To evaluate the good fitness of the EO-ANFIS model in the training phase, the MFs of the ANFIS model, after being optimised by the EO algorithm, was diagnosed, as shown in Figure 13. Accordingly, it is conspicuous that the shapes of the MFs after optimising by the EO algorithm are bell-shaped. Meanwhile, the shapes of MFs of the traditional ANFIS model are not normal, as depicted in Figures 8, 9, 10, 11. In other words, the mean and standard errors of the ANFIS model
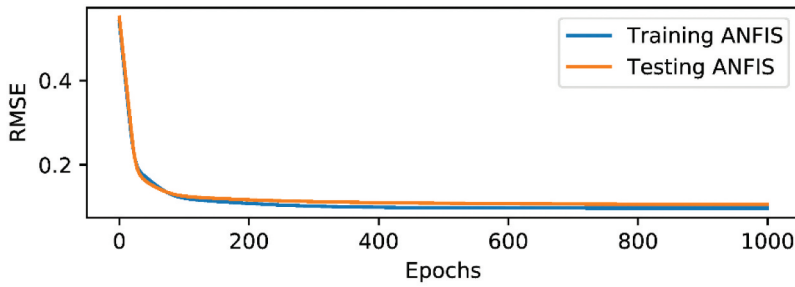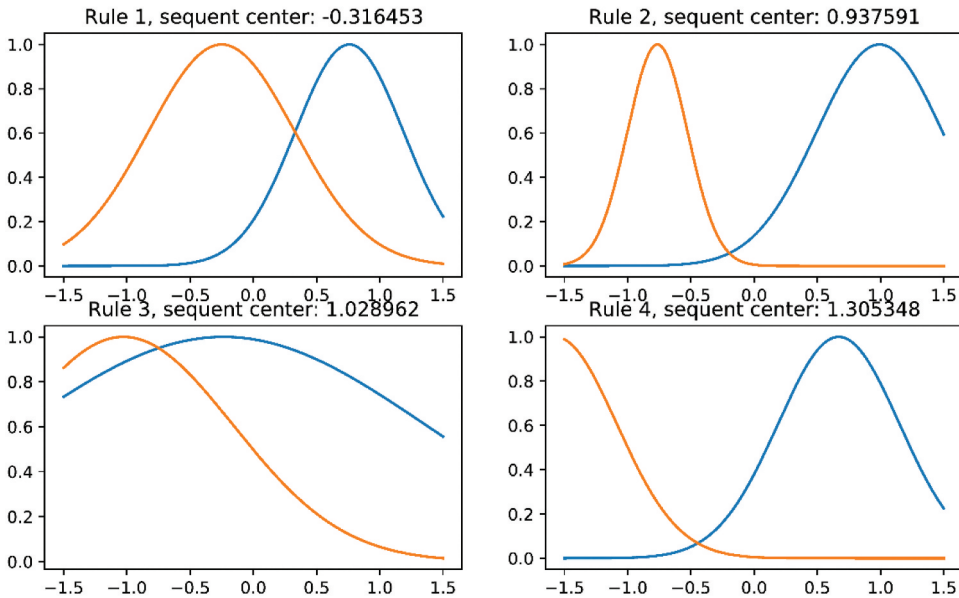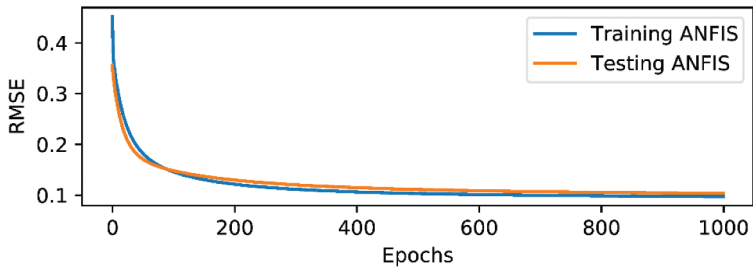
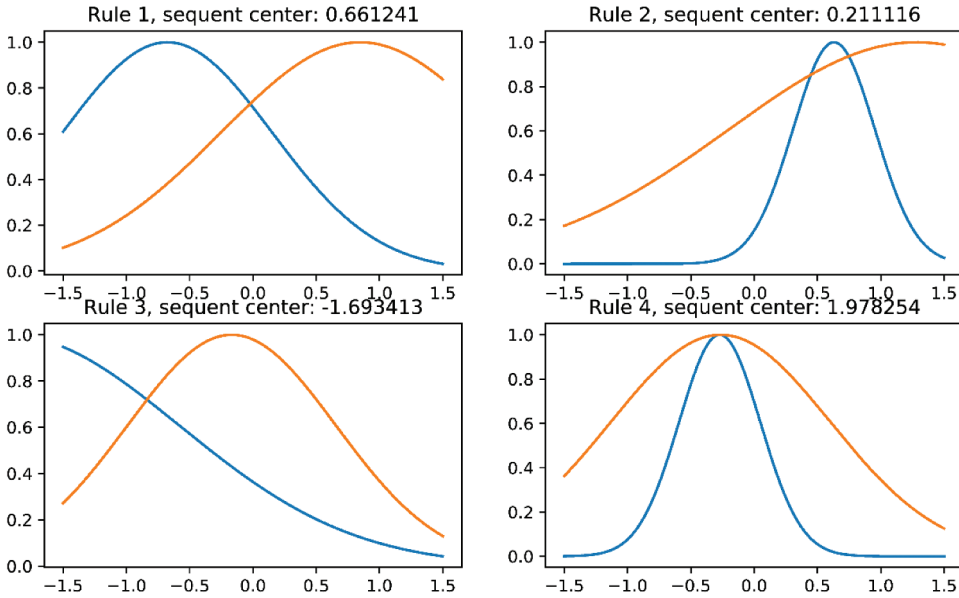**Figure 9.** Training performance and the accuracy of the ANFIS model for predicting transversal PPV.

are higher than the optimised EO-ANFIS model, and this finding was demonstrated through the prediction of PPV amplitude components. However, to have a good reason to interpret the effectiveness of the EO-ANFIS model, it needs to be further validated by the testing dataset and compared to the other models. These issues are presented and discussed in detail below paragraphs.

4.3. SVM model

In the SVM model, the kernel function is considered the main part of the model. The radial basis function was applied to determine the shape of the hyperplane and calculate the error from the datasets to the hyperplane through the support vectors. Accordingly, *sigma* (σ) and *cost* (c) were used to tune the performance of the SVM model through the RMSE and 10-fold cross-validation technique. A grid search with different values of σ (e.g. 0.025, 0.05, 0.075, 0.1) and c was set in the range of 1 to 50, as shown in Figure 14. The lowest RMSE values were selected as the best parameters of the SVM model for predicting PPV amplitude components.
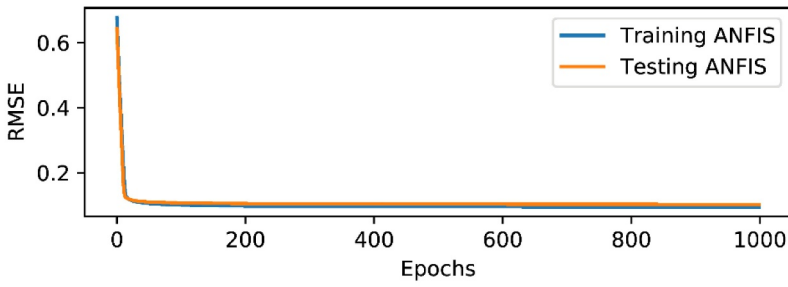
Figure 10. Training performance and the accuracy of the ANFIS model for predicting radial PPV (a) performance curves; (b) Trained MFs.

4.4. USBM model

This study selected the USBM model as the primary empirical model for predicting PPV values and compared it with the AI-based models. The formula of USBM was introduced by Duvall and Petkof [6], as described in Equation (14).

$$PPV = k\left(\frac{D}{\sqrt{W}}\right)^{-b} \tag{14}$$

where k and b are the site coefficients that the multivariate regression analysis can determine through the field measurements. Herein, various amplitude components of PPV were considered based on D and W. The empirical equations for these components finally are defined as described in Equations (15-18). The experimental PPV components as the functions of scaled distance are shown in Figure 15.
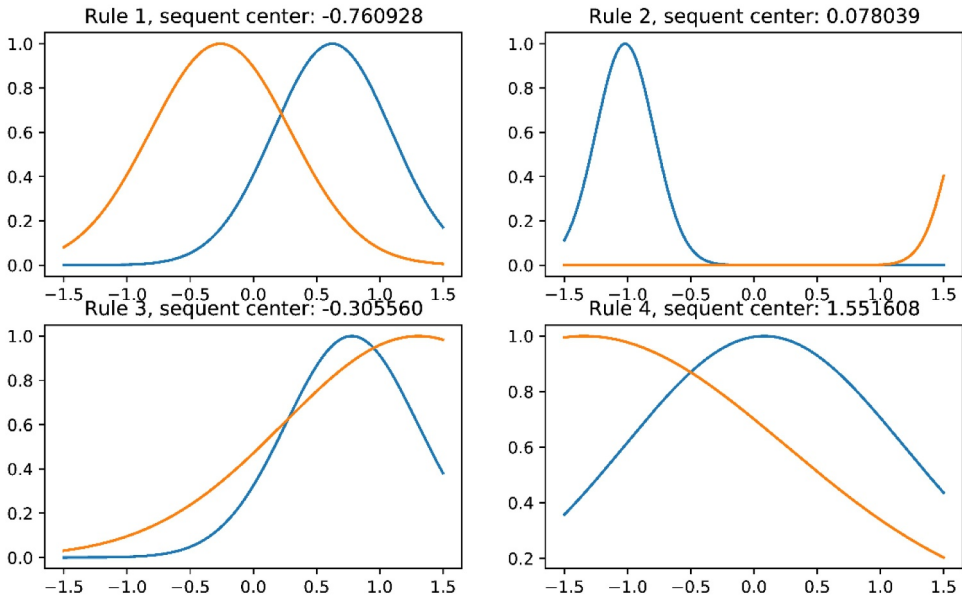
Figure 11. Training performance and the accuracy of the ANFIS model for predicting the vectoral sum of PPVs (a) performance curves; (b) Trained MFs.

$$PPV_{vertical} = 2219.373 \left(\frac{D}{\sqrt{W}} \right)^{-1.493} \tag{15}$$

$$PPV_{transversal} = 2217.421 \left(\frac{D}{\sqrt{W}} \right)^{-1.496} \tag{16}$$

$$PPV_{radial} = 2258.486 \left(\frac{D}{\sqrt{W}} \right)^{-1.501} \tag{17}$$

$$PPV_{sum} = 3848.351 \left(\frac{D}{\sqrt{W}} \right)^{-1.497} \tag{18}$$
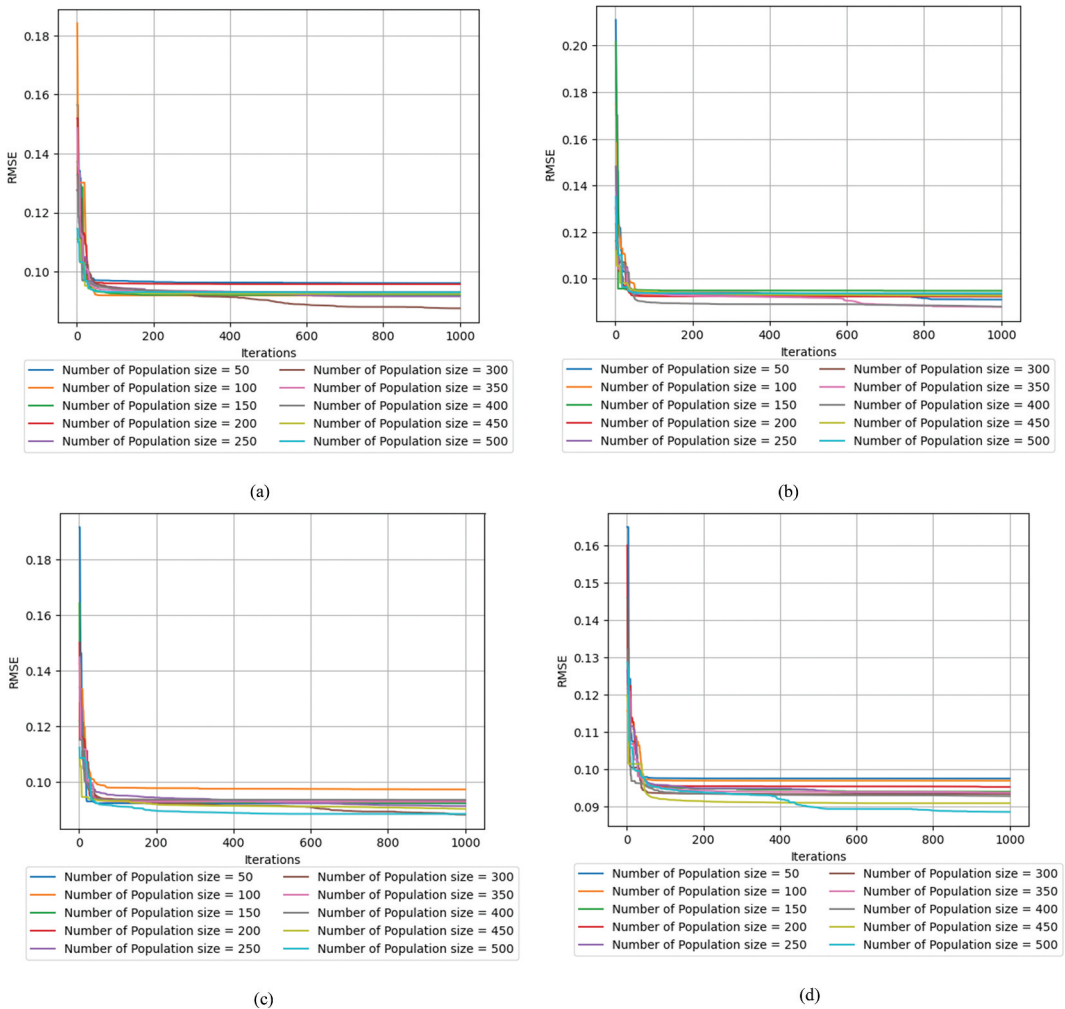
Figure 12. Training performance of the EO-ANFIS model for predicting PPV amplitude components (a) vertical PPV prediction; (b) transversal PPV prediction; (c) radial PPV prediction; (d) vectoral sum of PPV prediction.

4.5. Comparison and evaluation of the developed models

Predicting blast-induced PPV components is challenging due to the effects of uncontrollable parameters, e.g. geological and geographical conditions. Therefore, the PPV predictive models' accuracy is challenging for researchers worldwide. The development of the predictive models for PPV components based on the training dataset only provides the training point of view with insufficient. Therefore, evaluating the developed PPV predictive models based on the testing dataset is necessary to check whether the developed PPV models are good/valuable in practical engineering. Subsequently, they should be used to compare and select the best one among the developed models. The predicted PPV amplitude components by the individual models are shown in Figure 16.

The columns in Figure 16 indicate that the predicted PPV components by the EO-ANFIS model are more closely the measured PPV components than the other models. Remarkably, the shapes of the graphs are not too dissimilar. However, the range values of the PPV_sum are much larger than the three components separately. Consistency was also confirmed with the wide range of PPVs
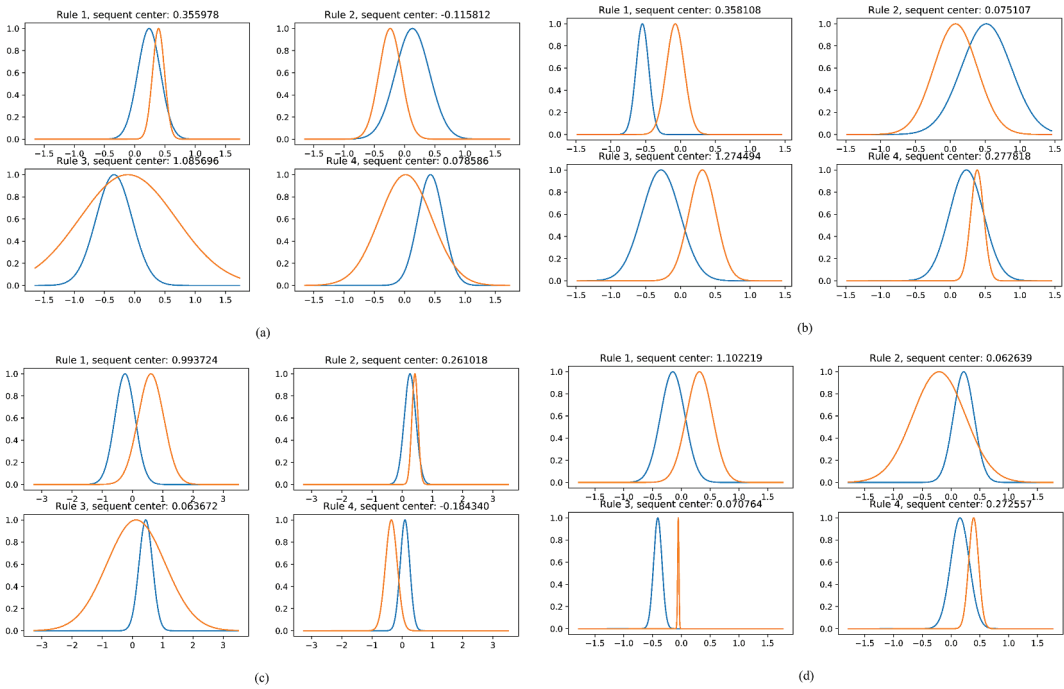
Figure 13. The shapes of the MFs optimized by the EO algorithm (a) optimized MFs of the PPV_ver; (b) optimized MFs of the PPV_trans; (c) optimized MFs of the PPV_rad; (d) optimized MFs of the PPV_sum.

based on the predicted PPV components by individual models. However, it is hard to determine which model best predicts various components. Therefore, statistical criteria are necessary and should be used to evaluate the performance of the developed models quantitatively. Herein, the accuracies and errors of the developed models were computed and evaluated through various statistical metrics, including RMSE, MAPE (mean absolute error), R2, and VAF (variance accounted for), as described in Equations (19-22). The computed statistical metrics are shown in Table 2.

$$\text{RMSE} = \sqrt{\frac{1}{n}\sum_{i=1}^{n}\left(y_{i\_PPVs} - \hat{y}_{i\_PPVs}\right)^2} \tag{19}$$

$$\text{MAPE} = \frac{1}{n}\sum_{i=1}^{n}\left|\frac{y_{i\_PPVs} - \hat{y}_{i\_PPVs}}{y_{i\_PPVs}}\right| \times 100\% \tag{20}$$

$$\text{R}^2 = 1 - \frac{\sum_i \left(y_{i\_PPVs} - \hat{y}_{i\_PPVs}\right)^2}{\sum_i \left(y_{i\_PPVs} - \bar{y}_{PPVs}\right)^2} \tag{21}$$

$$\text{VAF} = \left(1 - \frac{\text{var}\left(y_{i\_PPVs} - \hat{y}_{i\_PPVs}\right)}{\text{var}\left(y_{i\_PPVs}\right)}\right) \times 100 \tag{22}$$

Considering the criteria outlined in Table 2, a straightforward evaluation and comparison of the developed models' performance becomes feasible across each distinct PPV
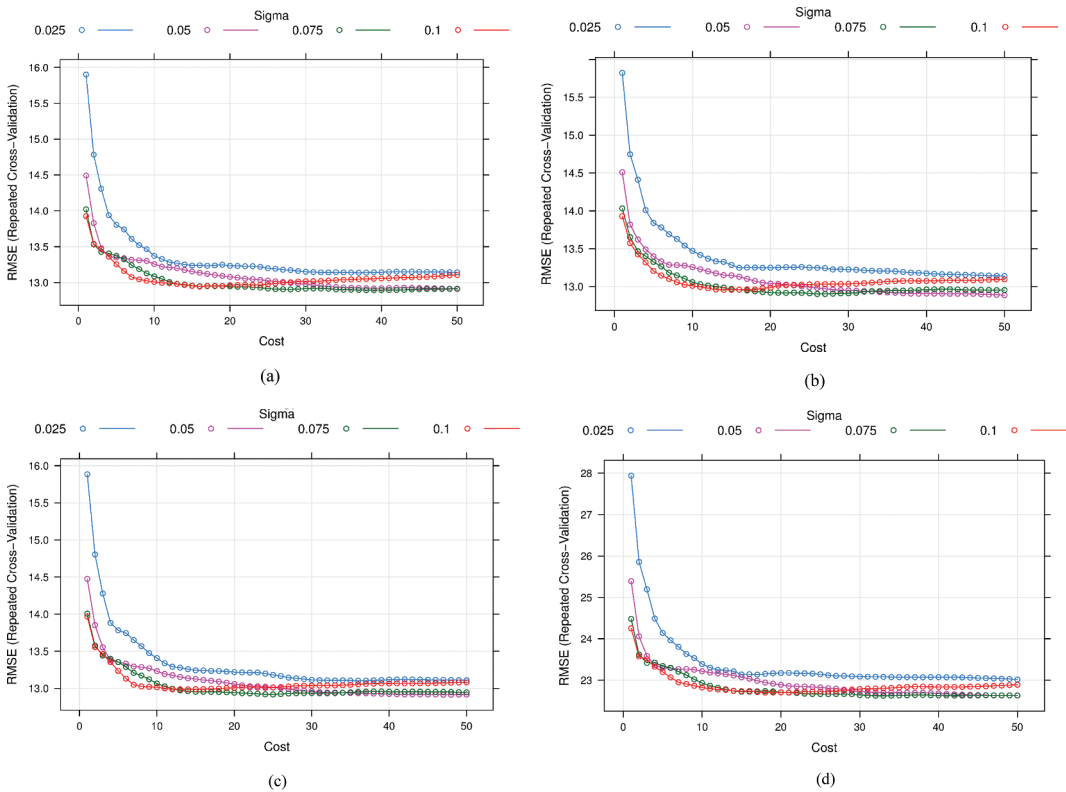
Figure 14. Training performance of the SVM model for predicting PPV amplitude components (a) vertical PPV; (b) transversal PPV; (c) radial PPV; (d) vectoral sum of PPVs.

component and the vectoral sum of PPVs. Upon scrutinising the model errors, which encompass RMSE and MAPE, for the separate prediction of the three components and the vectoral sum of PPVs, a noticeable pattern emerges: the errors linked to the models' PPV_sum predictions markedly surpass those associated with the prediction of the three individual components. To put it simply, the predictive models that focus on individual PPV components (namely, PPV_ver, PPV_rad, and PPV_trans) exhibit notably higher levels of accuracy than the models targeting the prediction of the vectoral sum of PPVs (PPV_sum). This revelation holds significance for mining companies and engineers, as it aids in the selection of the most suitable model for addressing a given PPV challenge within practical engineering contexts.

In the context of open-pit mines, only three distinct wave components were recorded for each blast, namely, PPV_ver, PPV_rad, and PPV_trans. Depending on geological conditions and rock properties, the intensity and frequency of these components can vary. Furthermore, their roles and intensities differ based on the relative positioning of buildings, benches, and slopes in relation to the blast site. In certain scenarios, vertical PPV exhibits the highest intensity, whereas in others, radial PPV takes precedence, as visually depicted in Figure 1. This multifaceted interplay underscores the complexities that must be considered for accurate predictive modelling in mining operations.

The primary objective of this study is to forecast various components of PPV resulting from open-pit mine blasting while assessing the accuracy of these predictions. As presented in Table 2, the EO-ANFIS model showcased the least errors across all PPV components, including PPV_sum. Impressively, its MAPE values lie within the narrow range of 0.398 to 0.4. It's noteworthy that
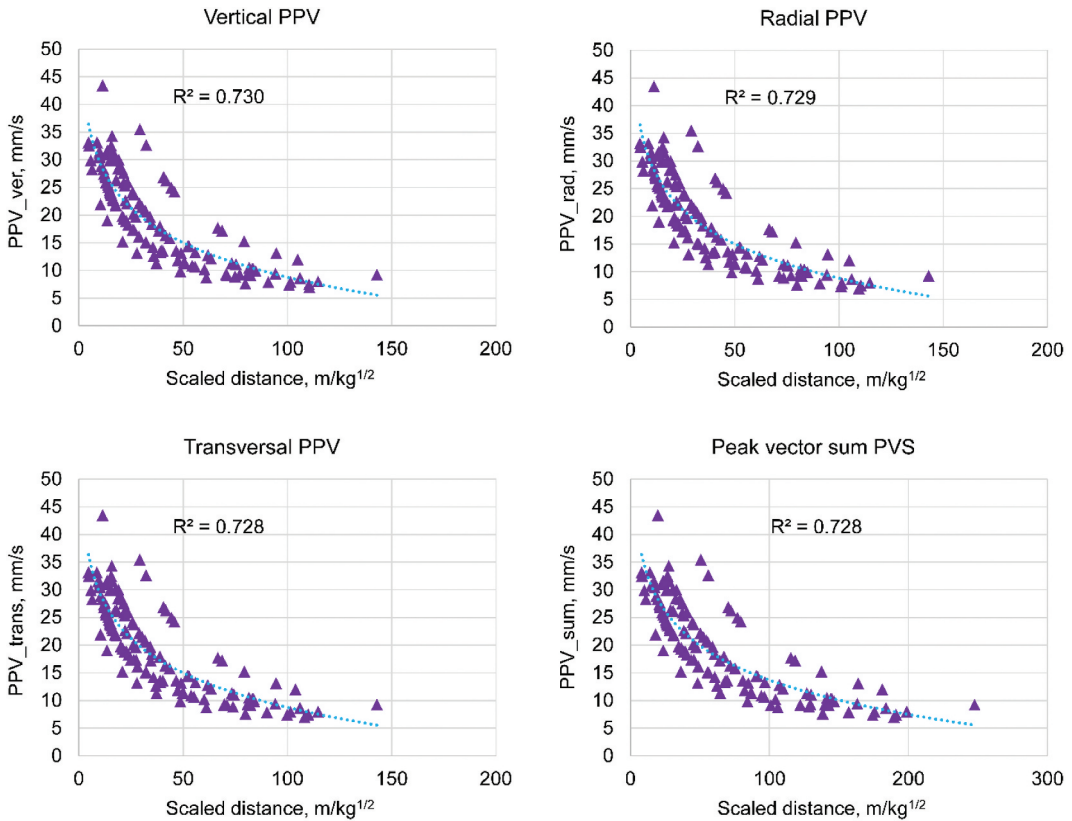
**Figure 15.** Experimental PPV components as the functions of scaled distance.

although the SVM and USBM models exhibit lower MAPE values than the EO-ANFIS model, their RMSE, R^2, and VAF metrics fall short of those achieved by the EO-ANFIS model.

Observing the performance of the ANFIS and EO-ANFIS models, it becomes evident that the EO algorithm significantly enhances the accuracy of the ANFIS model in predicting PPV components. Indeed, this improvement ranges from 5% to 8% when compared to the traditional ANFIS model in terms of PPV prediction. The optimisation outcomes are also vividly demonstrated in Figures 8 to 13. This reaffirms the robustness of the EO algorithm and its pivotal role in refining the precision of our predictive model.

In addition, considering the overfitting problem of the developed models, we need to observe consistent performance metrics between the training and testing datasets. Overfitting occurs when a model learns the training data too well, capturing noise and resulting in poor generalisation to new data. To determine the absence of overfitting, we look for similar or reasonably close values of these metrics between the two datasets for each model-amplitude component combination. Upon reviewing the results, we found that the RMSE, MAPE, R^2, and VAF values for each model and amplitude component are comparable between the training and testing datasets. This indicates that the models are not exhibiting significant discrepancies in their performance when applied to unseen data, thus suggesting that overfitting is not a prominent concern. Observing all the developed models for all components and their performance metrics on both training and testing datasets in Table 2, it is conspicuous that the consistent performance metrics across the training and testing datasets for this component and model demonstrate the model's robustness and its ability to generalise well to new data, indicating that overfitting is not an issue. Similarity in performance
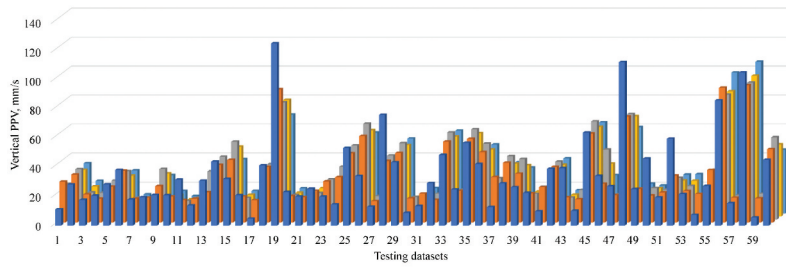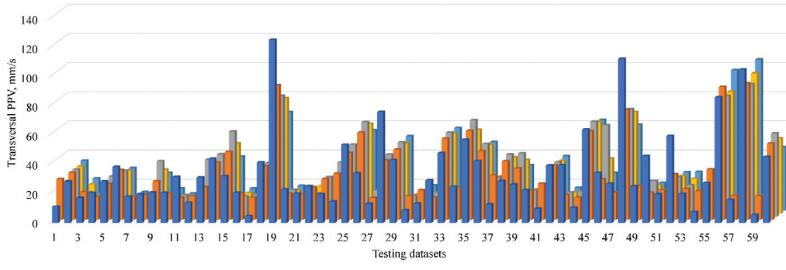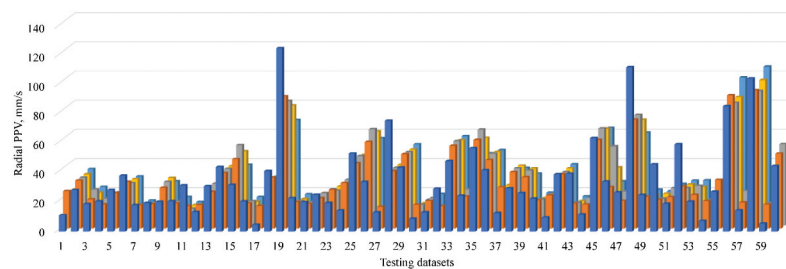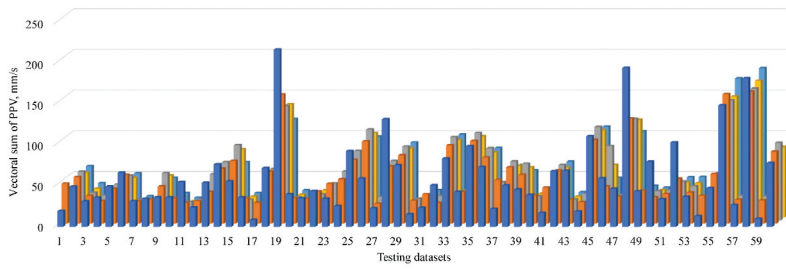
Figure 16. Comparisons of the actual and predicted PPV amplitude components (a) vertical PPV; (b) transversal PPV; (c) radial PPV; (d) vectoral sum of PPVs.

Table 2. The accuracies and errors of the AI and empirical models.

Amplitude component	Model	Training dataset				Testing dataset			
		RMSE	MAPE	R^2	VAF	RMSE	MAPE	R^2	VAF
PPV_ver	ANFIS	13.206	0.326	0.796	79.633	14.286	0.416	0.675	67.473
	EO-ANFIS	12.104	0.313	0.829	82.888	12.816	0.398	0.746	74.004
	SVM	12.891	0.322	0.810	81.063	14.090	0.367	0.705	70.126
	USBM	13.710	0.293	0.785	78.429	15.227	0.381	0.654	65.181
PPV_trans	ANFIS	13.402	0.329	0.788	78.827	14.670	0.427	0.657	65.675
	EO-ANFIS	12.159	0.313	0.826	82.572	12.859	0.403	0.743	73.785
	SVM	12.886	0.325	0.809	80.883	14.056	0.376	0.700	69.722
	USBM	13.768	0.296	0.781	78.073	15.323	0.382	0.651	64.919
PPV_rad	ANFIS	13.478	0.339	0.788	78.813	14.370	0.422	0.672	67.154
	EO-ANFIS	12.255	0.314	0.825	82.485	12.937	0.399	0.741	73.510
	SVM	12.914	0.333	0.810	80.081	14.011	0.375	0.698	69.684
	USBM	13.737	0.296	0.784	78.376	15.256	0.381	0.651	64.980
PPV_sum	ANFIS	22.882	0.322	0.795	79.476	24.714	0.413	0.676	67.535
	EO-ANFIS	21.218	0.315	0.824	82.355	22.314	0.400	0.744	73.732
	SVM	22.625	0.319	0.802	79.876	24.403	0.368	0.704	70.022
	USBM	24.018	0.297	0.779	77.817	26.519	0.379	0.652	65.009

metrics for both datasets across models and amplitude components affirms that the developed models are not suffering from overfitting and can provide reliable predictions when applied to unseen data.

To understand the distribution law of the predicted PPVs compared to the measured PPVs, Figure 17 shows their correlations with an 80% confidence level.

In Figure 17, the outcome predictions of PPV components were compared to the measured PPVs with an 80% confidence level. The PPVs predictions by the EO-ANFIS model are better than the other models, with the density of data points in the 80% confidence level being more significant than what the other models provided. Taking a closer look at the data points that outside of the 80% confidence level, most of the predicted PPVs by the EO-ANFIS model are more precise than those of the predicted PPVs by the other models. It is interesting to see that this dataset's recorded PPVs are in a wide range. However, the developed models worked well with such a wide range, as interpreted in Figure 17. Remarkably, the PPVs predictions in the range of 4.55 mm/s to 25 mm/s are outside the 80% confidence level (i.e. more significant than the measured PPVs) on all developed models. According to the recommendation of USBM, PPVs should not exceed 50.8 mm/s. Thus, given the safety aspect, the predictions in the range of 4.55 mm/s to 25 mm/s, with the errors of the developed models, are acceptable. However, in the viewpoint of the wasted explosive energy, this issue is still needed to consider and optimised to minimise the damage to the surroundings.

Considering the generalisability of the developed models for predicting PPV components, it is worth it if the percentage error (PE) and its frequency are evaluated in practical engineering. Therefore, the outcome predictions by the individual models were considered, and their PE was also calculated. Besides, the frequency of PE ranges was also analysed, as shown in Figure 18. Accordingly, the PE of the EO-ANFIS model is much better than the ANFIS, SVM, and USBM models in predicting PPV components, with most of the PEs in the low range. Meanwhile, the frequency of high errors of the ANFIS, SVM, and USBM models is larger than the EO-ANFIS model. Observing the PE of the predicted PPV components, we can see that some predicted values by the EO-ANFIS model are highest over the other models. However, considering the entire model with the whole testing dataset, it is clear that the PE of the EO-ANFIS model is smaller than the remaining models.

Based upon all the analysis and discussions, there are good reasons to believe that the EO-ANFIS model is the best paradigm to predict PPV components in the current study. The obtained results
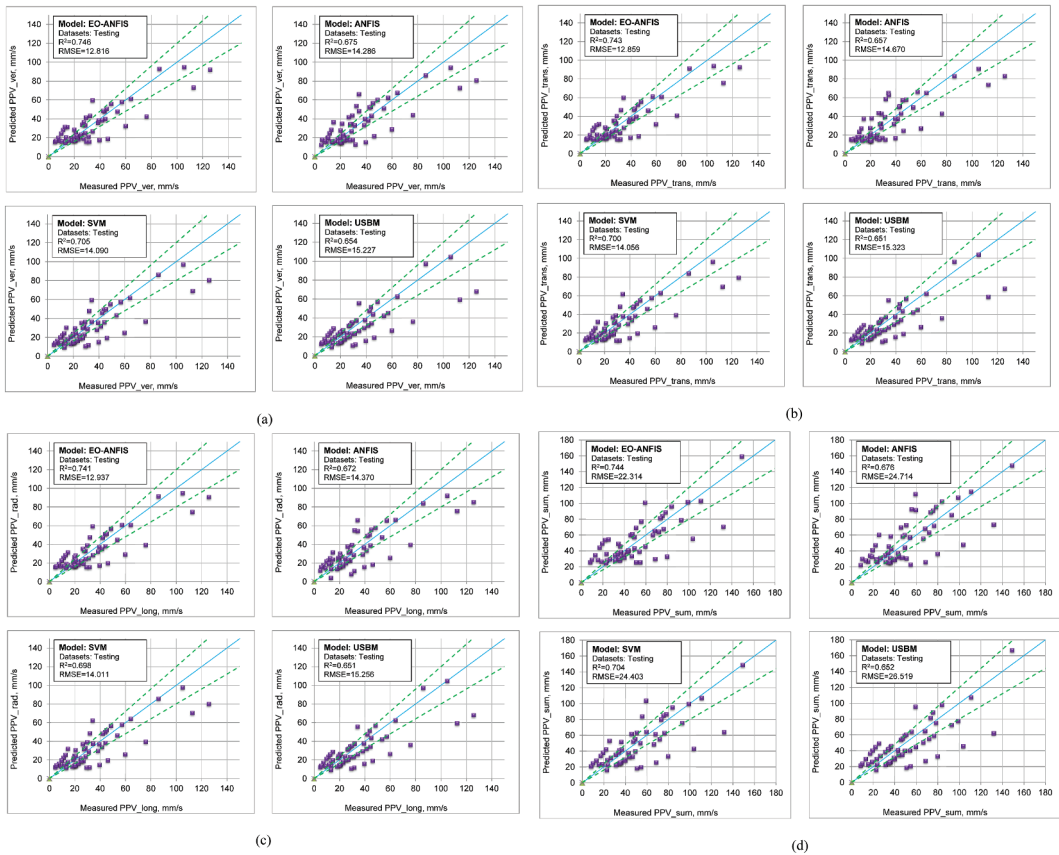
Figure 17. Measured versus predicted amplitude components of PPV (a) vertical PPV; (b) transversal PPV; (c) radial PPV; (d) vectoral sum of PPVs PVS.

demonstrated that its accuracy and reliability were improved significantly compared to the other AI models or the empirical model (i.e. the USBM model). Furthermore, using the EO-ANFIS model for predicting different PPV components is meaningful in practical engineering.

While the EO-ANFIS model proposed in this study is characterised as a black-box model, it can be conveniently exported as an API or a tool. This enables engineers and researchers to employ it for predicting PPV components in practical engineering applications, as illustrated in Figure 19. However, opening the inner workings of this black-box model, along with other analogous models in similar studies, remains a significant challenge. This opening could potentially assist engineers and researchers in optimising input parameters with the goal of minimising PPV components resulting from open-pit mine blasting.

5. Conclusion and remarks

Due to complex and ambiguous factors, PPV components are a considerable concern in open pit mines. A generalised model that can predict different PPV components with high accuracy and reliability is necessary for such open pit mines. Not only the PPV_sum is necessary to consider and predict, but also the other components (e.g. vertical PPV, radial PPV, transversal PPV) are necessary to take into account to have a strict control plan for PPV. This study considered different
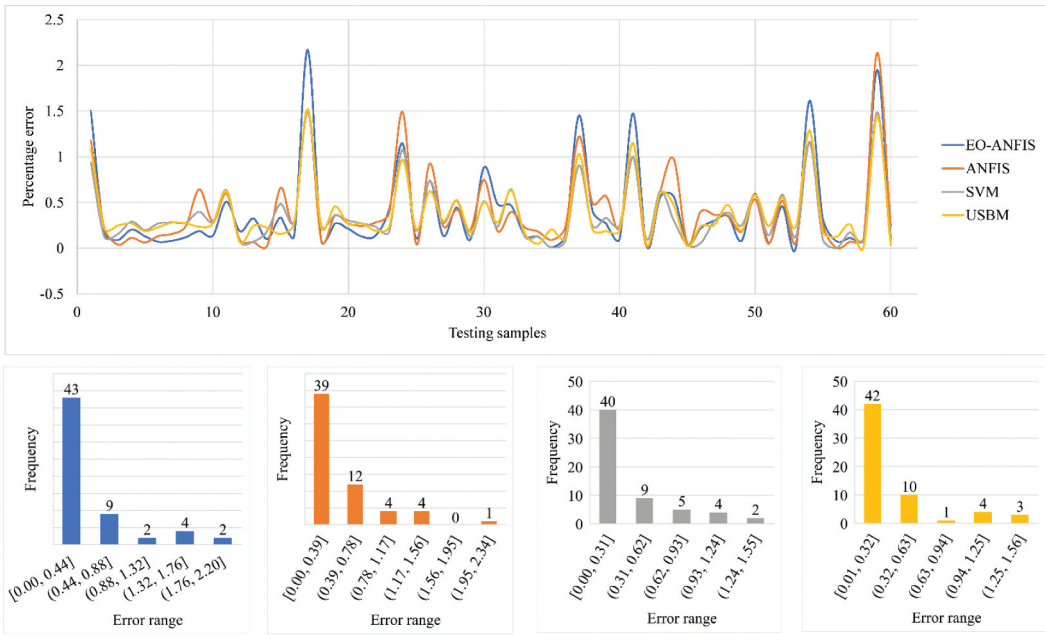
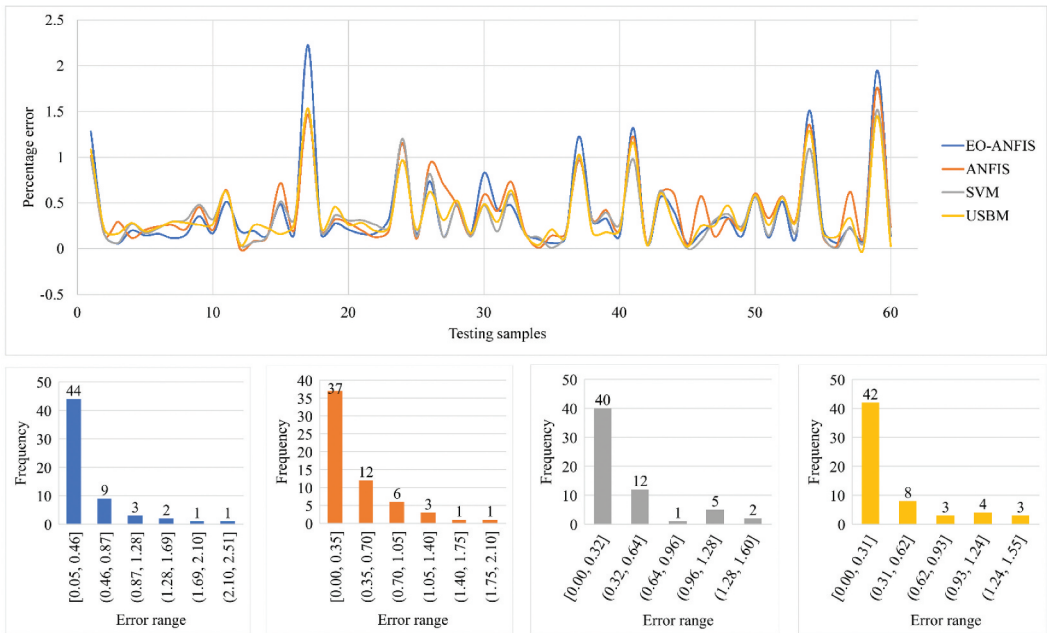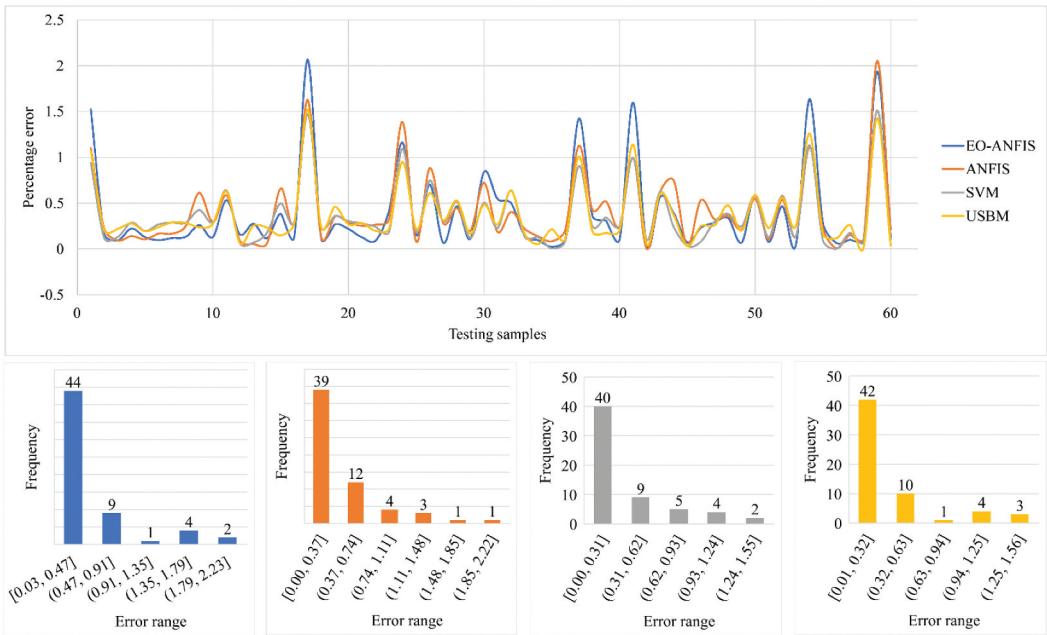(a)
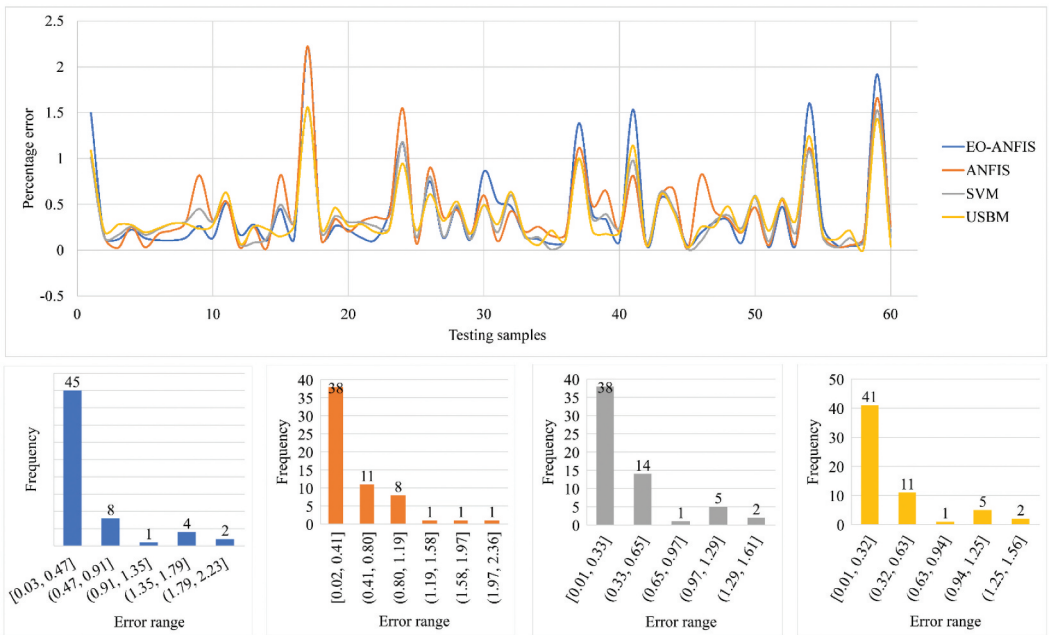
(b)

Figure 18. Percentage error of PPV amplitude components predictions and the histogram of percentage errors (a) vertical PPV; (b) transversal PPV; (c) radial PPV; (d) vectoral sum of PPVs PVS.

(c)
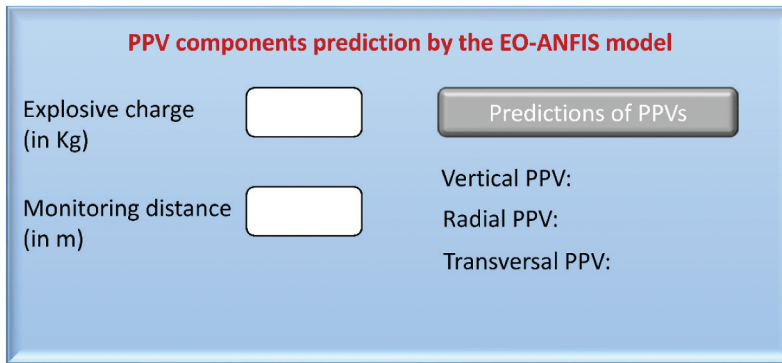

(d)

Figure 18. (Continued).

Figure 19. Utilize the implemented EO-ANFIS model as a predictive tool for real-world applications.

PPV components adequately and proposed a new soft computing model (i.e. EO-ANFIS) for predicting different PPV components. The empirical model (i.e. USBM) and other soft computing models (i.e. ANFIS, SVM) were also compared to the proposed EO-ANFIS model on all PPV components prediction. The following conclusions and remarks are drawn based on the obtained results of this study:

(1) The prediction models for three components of PPV provided higher accuracy than what they predicted for the Vectoral sum of PPVs.
(2) The AI models (i.e. ANFIS, SVM) are potential alternative solutions for predicting PPV components with higher accuracies.
(3) The EO algorithm is a robust optimisation solution to improve the accuracy of the ANFIS model for predicting PPV components in this study. The proposed EO-ANFIS model can be used as the generalised model for quarries in Nigeria.
(4) Other influential parameters should be investigated to enhance the PPV predictive models, aiming to prevent wasted explosive energy and harmful damage to nearby structures, including slopes in open pit mines.

Acknowledgments

Disclosure statement

No potential conflict of interest was reported by the authors.

ORCID

Hoang Nguyen http://orcid.org/0000-0001-6122-8314

Author contributions

Hoang Nguyen: Conceptualisation, Investigation, Methodology, Visualisation, Writing – Original Draft, Writing – Review & Editing, Project Administration, Revise the revision version.
Yosoon Choi, Masoud Monjezi, Nguyen Van Thieu, and Trung-Tin Tran: Conceptualisation, Methodology, Software, Formal Analysis, Writing – Review & Editing, Revise the revision version.

References

[1] H. Nguyen and X.-N. Bui, ANovel Hunger Games Search Optimization-Based Artificial Neural Network for Predicting Ground Vibration Intensity Induced by Mine Blasting, *Nat Resour Res*. 30 3865–3880. 2021. doi:10.1007/s11053-021-09903-8.

[2] A.Ö. Zgür and T. Taşkıran, *Investigation of blast-induced ground vibration effects on rural buildings*, Struct. Eng. Mech. 54 (3) (2015), pp. 545–560. doi:10.12989/sem.2015.54.3.545.

[3] M. Monjezi, M. Baghestani, R. Shirani Faradonbeh, M. Pourghasemi Saghand, and D. Jahed Armaghani, *Modification and prediction of blast-induced ground vibrations based on both empirical and computational techniques*, Eng. Comput 32 (4) (2016), pp. 717–728. doi:10.1007/s00366-016-0448-z.

[4] D. Huang, X. Qiu, X. Shi, Y. Gou, and J. Zhou, *Experimental and numerical investigation of blast-induced vibration for short-delay cut blasting in underground mining*, Shock Vib. 2019 (2019), pp. 1–13. doi:10.1155/2019/5843516.

[5] R. Kumar, D. Choudhury, and K. Bhargava, *Determination of blast-induced ground vibration equations for rocks using mechanical and geological properties*, J. Rock Mech. Geotech. Eng. 8 (3) (2016), pp. 341–349. doi:10.1016/j.jrmge.2015.10.009.

[6] W.I. Duvall and B. Petkof, *Spherical Propagation of Explosion-Generated Strain Pulses in Rock, US Department of the Interior*, Washington, D.C: Bureau of Mines, 1959.

[7] U. Langefors and B. Kihlström, *The Modern Technique of Rock Blasting*, University of California: Wiley, 1963.

[8] N. Ambraseys and A. Hendron, *Dynamic Behavior of Rock Masses in Rock Mechanics in Engineering Practice*, KG Stagg & OC Zienkievicz, Eds., John Wiley and Sons, New York, 1968, pp. 203–207.

[9] A. Ghosh and J.J. Daemen, *A simple new blast vibration predictor (based on wave propagation laws)*, in *The 24th US Symposium on Rock Mechanics (USRMS)*, American Rock Mechanics Association, College Station, Texas, 1983. https://onepetro.org/ARMAUSRMS/ARMA83/conference/All-ARMA83.

[10] P.P. Roy, *Prediction and control of ground vibration due to blasting*, Colliery Guardian 239 (1991), pp. 215–219.

[11] W.S. Iramina, E.C. Sansone, M. Wichers, S. Wahyudi, S.M.D. Eston, H. Shimada, and T. Sasaoka, *Comparing blast-induced ground vibration models using ANN and empirical geomechanical relationships*, Int. Eng. J 71 (2018), pp. 89–95.

[12] S. Kostić, M. Perc, N. Vasović, S. Trajković, and T. Preis, *Predictions of experimentally observed stochastic ground vibrations induced by blasting*, PLoS One 8 (12) (2013), pp. e82056. doi:10.1371/journal.pone.0082056.

[13] Q. Fang, H. Nguyen, X.-N. Bui, and T. Nguyen-Thoi, *Prediction of blast-induced ground vibration in open-pit mines using a new technique based on imperialist competitive algorithm and M5Rules*, Nat. Resour. Res. 29 (2) (2020), pp. 791–806. doi:10.1007/s11053-019-09577-3.

[14] M. Hasanipanah, M. Monjezi, A. Shahnazar, D.J. Armaghani, and A. Farazmand, *Feasibility of indirect determination of blast induced ground vibration based on support vector machine*, Measurement 75 (2015), pp. 289–297. doi:10.1016/j.measurement.2015.07.019.

[15] R.S. Faradonbeh and M. Monjezi, *Prediction and minimization of blast-induced ground vibration using two robust meta-heuristic algorithms*, Eng. Comput 33 (4) (2017), pp. 835–851. doi:10.1007/s00366-017-0501-6.

[16] M. Amiri, H.B. Amnieh, M. Hasanipanah, and L.M. Khanli, *A new combination of artificial neural network and K-nearest neighbors models to predict blast-induced ground vibration and air-overpressure*, Eng. Comput 32 (4) (2016), pp. 631–644. doi:10.1007/s00366-016-0442-5.

[17] M. Hasanipanah, R.S. Faradonbeh, H.B. Amnieh, D.J. Armaghani, and M. Monjezi, *Forecasting blast-induced ground vibration developing a CART model*, Eng. Comput 33 (2) (2017), pp. 307–316. doi:10.1007/s00366-016-0475-9.

[18] Y. Shang, H. Nguyen, X.-N. Bui, Q.-H. Tran, and H. Moayedi, *A novel artificial intelligence approach to predict blast-induced ground vibration in open-pit mines based on the Firefly algorithm and artificial neural network*, Nat. Resour. Res. 29 (2) (2019), pp. 723–737. doi:10.1007/s11053-019-09503-7.

[19] W. Chen, M. Hasanipanah, H.N. Rad, D.J. Armaghani, and M. Tahir, *A new design of evolutionary hybrid optimization of SVR model in predicting the blast-induced ground vibration*, Eng. Comput. 37 (2021), pp. 1455–1471. doi:10.1007/s00366-019-00895-x.

[20] Van Thieu N and Mirjalili S. MEALPY: An open-source library for latest meta-heuristic algorithms in Python. Journal of Systems Architecture, 139 (2023), 102871. doi:10.1016/j.sysarc.2023.102871.

[21] Nguyen, Thieu, Nhuan Tran, Binh Minh Nguyen, and Giang Nguyen. "A resource usage prediction system using functional-link and genetic algorithm neural network for multivariate cloud metrics." In 2018 IEEE 11th conference on service-oriented computing and applications (SOCA), pp. 49–56. (2018). IEEE. doi:10.1109/SOCA.2018.00014.

[22] C.K. Arthur, V.A. Temeng, and Y.Y. Ziggah, *Novel approach to predicting blast-induced ground vibration using Gaussian process regression*, Eng. Comput 36 (1) (2020), pp. 29–42. doi:10.1007/s00366-018-0686-3.

[23] Van Thieu N, Deb Barma S, Van Lam T, Kisi O and Mahesha A. Groundwater level modeling using Augmented Artificial Ecosystem Optimization. Journal of Hydrology, 617, (2023), 129034. doi:10.1016/j. jhydrol.2022.129034.

[24] Nguyen, Thieu, Giang Nguyen, and Binh Minh Nguyen. "EO-CNN: an enhanced CNN model trained by equilibrium optimization for traffic transportation prediction." Procedia Computer Science, 176 (2020), 800–809. doi:10.1016/j.procs.2020.09.075.

[25] Ahmed A Najah, Van Lam T, Hung N Duy, Van Thieu N, Kisi O and El-Shafie A. A comprehensive comparison of recent developed meta-heuristic algorithms for streamflow time series forecasting problem. Applied Soft Computing, 105 (2021), 107282. doi:10.1016/j.asoc.2021.107282.

[26] Y. Qiu, J. Zhou, M. Khandelwal, H. Yang, P. Yang, and C. Li, *Performance evaluation of hybrid WOA-XGBoost, GWO-XGBoost and BO-XGBoost models to predict blast-induced ground vibration*, Eng. Comput 38 (S5) (2022), pp. 4145–4162. doi:10.1007/s00366-021-01393-9.

[27] D.J. Armaghani, D. Kumar, P. Samui, M. Hasanipanah, and B. Roy, *A novel approach for forecasting of ground vibrations resulting from blasting: Modified particle swarm optimization coupled extreme learning machine*, Eng. Comput 37 (4) (2021), pp. 3221–3235. doi:10.1007/s00366-020-00997-x.

[28] X.-N. Bui, H. Nguyen, Q.H. Tran, D.A. Nguyen, and H.B. Bui, *Predicting ground vibrations due to mine blasting using a novel artificial neural network-based Cuckoo search optimization*, Nat. Resour. Res. 30 (3) (2021), pp. 2663–2685. doi:10.1007/s11053-021-09823-7.

[29] X.-N. Bui, H. Nguyen, Q.-H. Tran, D.A. Nguyen, and H.B. Bui, *Predicting blast-induced ground vibration in quarries using adaptive fuzzy inference neural network and Moth–Flame optimization*, Nat. Resour. Res. 30 (6) (2021), pp. 4719–4734. doi:10.1007/s11053-021-09968-5.

[30] H. Fattahi and M. Hasanipanah, *Prediction of blast-induced ground vibration in a mine using Relevance vector regression optimized by metaheuristic algorithms*, Nat. Resour. Res. 30 (2) (2021), pp. 1849–1863. doi:10.1007/s11053-020-09764-7.

[31] B. Ke, H. Nguyen, X.-N. Bui, and R. Costache, *Estimation of ground vibration intensity induced by mine blasting using a state-of-the-Art hybrid Autoencoder neural network and support vector regression model*, Nat. Resour. Res. 30 (5) (2021), pp. 3853–3864. doi:10.1007/s11053-021-09890-w.

[32] A.I. Lawal, S. Kwon, O.S. Hammed, and M.A. Idris, *Blast-induced ground vibration prediction in granite quarries: An application of gene expression programming, ANFIS, and sine cosine algorithm optimized ANN*, Int. J. Min. Sci. Technol. 31 (2) (2021), pp. 265–277. doi:10.1016/j.ijmst.2021.01.007.

[33] H. Nguyen and X.-N. Bui, *A novel Hunger Games search optimization-based artificial neural network for predicting ground vibration intensity induced by mine blasting*, Nat. Resour. Res. 30 (5) (2021), pp. 3865–3880. doi:10.1007/s11053-021-09903-8.

[34] H. Nguyen, X.-N. Bui, Q.-H. Tran, D.-A. Nguyen, L.T.T. Hoa, Q.-T. Le, and L.T.H. Giang, *Predicting blast-induced ground vibration in open-pit mines using different nature-inspired optimization algorithms and Deep neural network*, Nat. Resour. Res. 30 (6) (2021), pp. 4695–4717. doi:10.1007/s11053-021-09896-4.

[35] H. Nguyen, X.-N. Bui, Q.-H. Tran, H.A. Nguyen, D.-A. Nguyen, and Q.-T. Le, *Prediction of ground vibration intensity in mine blasting using the novel hybrid MARS–PSO–MLP model*, Eng. Comput 38 (S5) (2021), pp. 1–19. doi:10.1007/s00366-021-01332-8.

[36] K. Peng, J. Zeng, D.J. Armaghani, M. Hasanipanah, and Q. Chen, *A novel combination of gradient Boosted Tree and optimized ANN models for forecasting ground vibration due to quarry blasting*, Nat. Resour. Res. 30 (6) (2021), pp. 1–15. doi:10.1007/s11053-021-09899-1.

[37] Y. Qiu, J. Zhou, M. Khandelwal, H. Yang, P. Yang, and C. Li, *Performance evaluation of hybrid WOA-XGBoost, GWO-XGBoost and BO-XGBoost models to predict blast-induced ground vibration*, Eng. Comput. 38 (Suppl 5), 4145–4162. (2022). doi:10.1007/s00366-021-01393-9.

[38] J. Zhou, Y. Qiu, M. Khandelwal, S. Zhu, and X. Zhang, *Developing a hybrid model of Jaya algorithm-based extreme gradient boosting machine to estimate blast-induced ground vibrations*, Int. J. Rock Mech. Min. Sci. 145 (2021), pp. 104856. doi:10.1016/j.ijrmms.2021.104856.

[39] W. Zhu, H. Nikafshan Rad, and M. Hasanipanah, *A chaos recurrent ANFIS optimized by PSO to predict ground vibration generated in rock blasting*, Appl. Soft. Comput. 108 (2021), pp. 107434. doi:10.1016/j.asoc.2021.107434.

[40] D.J. Armaghani, M. Hasanipanah, H.B. Amnieh, and E.T. Mohamad, *Feasibility of ICA in approximating ground vibration resulting from mine blasting*, Neural Comput. Appl 29 (9) (2018), pp. 457–465. doi:10.1007/s00521-016-2577-0.

[41] D.J. Armaghani, M. Hajihassani, E.T. Mohamad, A. Marto, and S. Noorani, *Blasting-induced flyrock and ground vibration prediction through an expert artificial neural network based on particle swarm optimization*, Arab. J. Geosci. 7 (12) (2014), pp. 5383–5396. doi:10.1007/s12517-013-1174-0.

[42] G.-G. Wang, S. Deb, and L.D.S. Coelho, *Earthworm optimisation algorithm: A bio-inspired metaheuristic algorithm for global optimisation problems*, Int. J. Bio-Inspired Comput. 12 (1) (2018), pp. 1–22. doi:10.1504/IJBIC.2018.093328.

[43] S. Kirkpatrick, C.D. Gelatt, and M.P. Vecchi, *Optimization by simulated annealing*, Science 220 (4598) (1983), pp. 671–680. doi:10.1126/science.220.4598.671.

[44] U. Çaydaş, A. Hasçalık, and S. Ekici, *An adaptive neuro-fuzzy inference system (ANFIS) model for wire-EDM*, Expert Syst. Appl 36 (3) (2009), pp. 6135–6139. doi:10.1016/j.eswa.2008.07.019.

[45] V. Padmajothi and J. Iqbal, *Adaptive neural fuzzy inference system-based scheduler for cyber–physical system*, Soft Comput. 24 (22) (2020), pp. 17309–17318. doi:10.1007/s00500-020-05020-5.

[46] S. Bahl, S. Singh, P. Goyal, and A.K. Bagha, *Experimental investigations on brass material and pin–fin based heat transfer system and its modeling by using adaptive neuro-fuzzy inference system*, Mater. Today Proc. 45 (2021), pp. 5323–5327.

[47] H. Karimi, M.T.H. Beheshti, A. Ramezani, and H. Zareipour, *Intelligent control of islanded AC microgrids based on adaptive neuro-fuzzy inference system*, Int. J. Elec. Power 133 (2021), pp. 107161. doi:10.1016/j.ijepes.2021.107161.

[48] A.T. Owoseni, O. Olabode, K.G. Akintola, and P.A. Enikanselu, *An improved adaptive neuro-fuzzy inference system using probability trajectory-based clustering ensemble*, Sci. Afr. 9 (2020), pp. e00520. doi:10.1016/j.sciaf.2020.e00520.

[49] M. Phate, A. Bendale, S. Toney, and V. Phate, *Prediction and optimization of tool wear rate during electric discharge machining of Al/Cu/Ni alloy using adaptive neuro-fuzzy inference system*, Heliyon 6 (10) (2020), pp. e05308. doi:10.1016/j.heliyon.2020.e05308.

[50] M. Zeinalnezhad, A.G. Chofreh, F.A. Goni, and J.J. Klemeš, *Air pollution prediction using semi-experimental regression model and adaptive neuro-fuzzy inference System*, J. Clean. Prod. 261 (2020), pp. 121218. doi:10.1016/j.jclepro.2020.121218.

[51] O. Hammed, O. Popoola, A. Adetoyinbo, M. Awoyemi, T. Adagunodo, O. Olubosede, and A. Bello, *Peak particle velocity data acquisition for monitoring blast induced earthquakes in quarry sites*, Data Brief 19 (2018), pp. 398–408. doi:10.1016/j.dib.2018.04.103.

[52] P. Melin, J. Soto, O. Castillo, and J. Soria, *A new approach for time series prediction using ensembles of ANFIS models*, Expert Syst. Appl 39 (3) (2012), pp. 3494–3506. doi:10.1016/j.eswa.2011.09.040.